



저작자표시-비영리-변경금지 2.0 대한민국

이용자는 아래의 조건을 따르는 경우에 한하여 자유롭게

- 이 저작물을 복제, 배포, 전송, 전시, 공연 및 방송할 수 있습니다.

다음과 같은 조건을 따라야 합니다:



저작자표시. 귀하는 원저작자를 표시하여야 합니다.



비영리. 귀하는 이 저작물을 영리 목적으로 이용할 수 없습니다.



변경금지. 귀하는 이 저작물을 개작, 변형 또는 가공할 수 없습니다.

- 귀하는, 이 저작물의 재이용이나 배포의 경우, 이 저작물에 적용된 이용허락조건을 명확하게 나타내어야 합니다.
- 저작권자로부터 별도의 허가를 받으면 이러한 조건들은 적용되지 않습니다.

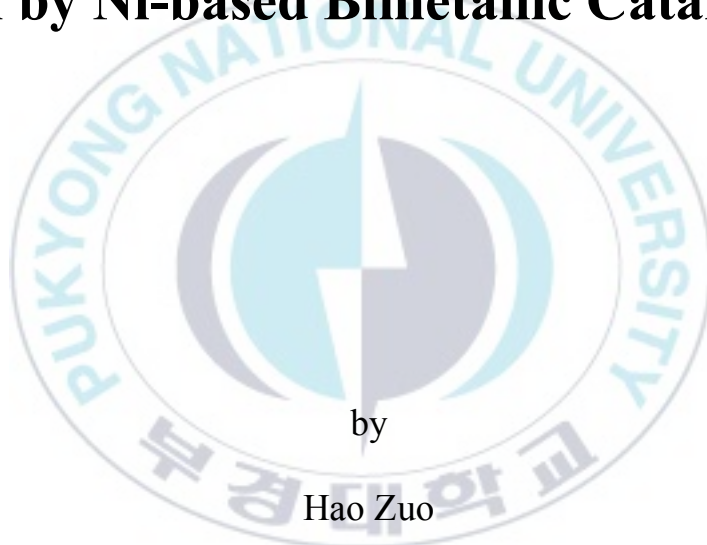
저작권법에 따른 이용자의 권리는 위의 내용에 의하여 영향을 받지 않습니다.

이것은 [이용허락규약\(Legal Code\)](#)을 이해하기 쉽게 요약한 것입니다.

[Disclaimer](#)

Thesis for the Degree of Master of Engineering

Hydrogenation of Non-edible Vegetable Oil by Ni-based Bimetallic Catalysts



by

Hao Zuo

Department of Chemical Engineering

The Graduate School

Pukyong National University

August, 2018

Hydrogenation of Non-edible Vegetable Oil by Ni-based Bimetallic Catalysts

니켈계 이원금속촉매에 의한 비식용 식물유의 수소화 반응

Advisor: Prof. Hee Chul Woo

by

Hao Zuo

A thesis submitted in partial fulfillment of the requirements
for the degree of

Master of Engineering

in Department of Chemical Engineering, The Graduate School,
Pukyong National University

August 2018

**Hydrogenation of Non-edible Vegetable Oil by Ni-based
Bimetallic Catalysts**

A dissertation

by

Hao Zuo

Approved by:



(Chairman) Jun Heok Lim



(Member) Jay Liu



(Member) Hee Chul Woo

August 24, 2018

CONTENTS

CONTENTS	i
ABSTRACT	iv
LIST OF TABLES	vii
LIST OF FIGURES	viii
1. INTRODUCTION	1
1.1. Research background.....	1
1.2. Literature review	6
1.2.1. Feedstocks: CNSL and PAO.....	6
1.2.2. Hydrogenation.....	11
1.2.3. Catalysts.....	12
1.3. Objectives	13
2. MATERIALS AND EXPERIMENTAL	14
2.1. Materials	14
2.2. Catalyst preparation.....	14

2.3. Catalyst characterization.....	18
2.3.1. Brunauer-Emmett-Teller (BET).....	18
2.3.2. X-ray fluorescence (XRF)	18
2.3.3. X-ray diffraction (XRD).....	19
2.3.4. X-ray photoelectron spectroscopy (XPS)	19
2.4. Catalytic upgrading	20
2.5. Analysis of upgraded oil.....	23
3. RESULTS AND DISCUSSIONS	25
3.1. Catalyst characterization.....	25
3.1.1. Brunauer-Emmett-Teller (BET).....	25
3.1.2. X-ray fluorescence (XRF)	27
3.1.3. X-ray diffraction (XRD)	29
3.1.4. X-ray photoelectron spectroscopy (XPS)	37
3.2. Catalytic activity test	41
3.2.1. Screening test for bimetal effect.....	41
3.2.2. NiCu/ γ -Al ₂ O ₃ : reaction condition effect.....	43

3.2.2.1. NiCu/ γ -Al ₂ O ₃ : temperature effect.....	43
3.2.2.2. NiCu/ γ -Al ₂ O ₃ : pressure effect	45
3.2.2.3. NiCu/ γ -Al ₂ O ₃ : LHSV effect.....	47
3.2.2.4. NiCu/ γ -Al ₂ O ₃ : Cu contents effect.....	49
3.2.3. Longevity test	51
3.3. Study of catalyst deactivation	53
4. CONCLUSIONS.....	55
ABSTRACT IN KOREAN.....	58
REFERENCES.....	58
ACKNOWLEDGEMENT.....	66

Hydrogenation of Non-edible Vegetable Oil by Ni-based Bimetallic Catalysts

Hao Zuo

Department of Chemical Engineering, The Graduate School,
Pukyong National University

Abstract

Non-edible vegetable oil can be considered as a promising alternative energy source to replace the limited amounts of fossil fuels for power generation. However, the fuel quality of non-edible vegetable oil is inferior to that of fossil fuels, and its high acidity and high degree of unsaturation give rise to corrosiveness and undesirable polymerization reactions during storage. The catalytic hydrogenation process is a promising path by which to upgrade vegetable oil. At present, Ni-based bimetallic catalysts containing NiZn/Al₂O₃ and NiFe/Al₂O₃ have attracted a great deal of attention due to their excellent catalytic activity and stability levels.

In this study, non-edible vegetable oil hydrogenation over NiM/ γ -Al₂O₃ bimetallic catalysts was investigated to assess the effects of the bimetal type, bimetal contents and reaction conditions. To evaluate the extent of upgraded oil, the iodine value (IV) and the total acid number (TAN) were analyzed. γ -Al₂O₃ supported NiM/ γ -Al₂O₃ (M₁=Zn, Fe, Cu and Co, 15 wt% Ni, Ni/M₁ molar ratio=2/1; M₂=Pd and Pt, 15 wt% Ni, Ni/M₂ molar ratio=20/1) bimetallic catalysts were prepared by a co-impregnation method and characterized by BET, XRF, XRD and XPS. Screening tests of the bimetal catalysts were conducted under the condition of 350 °C, 30 bar and LHSV=1 h⁻¹ in a packed-bed reactor. The NiCu/ γ -Al₂O₃ catalyst was selected as a promising catalyst, and the activity test was performed under a range of temperatures (250-400 °C), pressures (5-80 bar) and LHSVs (1-10 h⁻¹). In addition, the influence of NiCu bimetal content (0-23 wt% in the catalyst) was assessed, and a longevity test was also conducted. A 1/1 (v/v %) mixture of cashew nut shell liquid (CNSL) and palm acid oil (PAO) was selected as the feed

(IV:186.30, TAN:42.90).

In the activity test, NiCu/ γ -Al₂O₃ was found to enhance the catalytic performance considerably with the synergistic effect between nickel and copper. The best catalyst, Ni(18.1)Cu(4.9)/ γ -Al₂O₃ (Ni/Cu molar ratio=4/1), showed that the IV and TAN removal efficiency rates could reach 81.5% and 100.0%, respectively, at 350 °C, 30 bar, and LHSV=1 h⁻¹. Overall, the unsaturated double bonds and the carboxylic acid from non-edible vegetable oil showed significant decreases by the hydrogenation process over the NiCu/ γ -Al₂O₃ bimetallic catalyst.

LIST OF TABLES

Table 1.1.	The quality standards of bio-fuel for power generation.	5
Table 1.2.	The Compositions of FFA in PAO.	9
Table 1.3.	The physicochemical characteristics of CNSL and PAO.	10
Table 3.1.	Textural properties of different synthesized catalysts.	26
Table 3.2.	XRF data of different synthesized catalysts.	28
Table 3.3.	Crystallite size obtained from reduced and spent NiCu/ γ -Al ₂ O ₃ catalysts.	36
Table 3.4.	ICP-AES data of feedstock and Ni(18.1)Cu(4.9)/ γ -Al ₂ O ₃ catalyst.	54

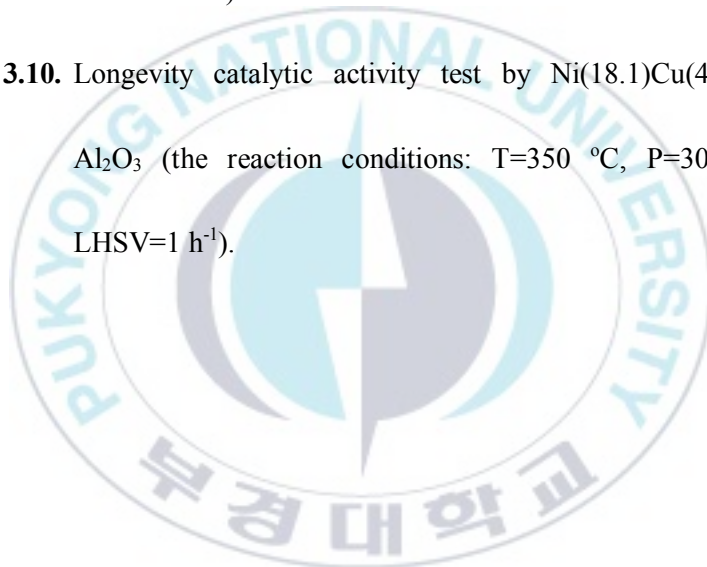
LIST OF FIGURES

- Fig. 1.1.** The structures of CNSL constituents. 8
- Fig. 2.1.** The preparation procedure of bimetallic catalysts. 17
- Fig. 2.2.** The schematic diagram of packed-bed reactor. 22
- Fig. 3.1.** The XRD patterns of different bimetal types for NiM/ γ - Al_2O_3 . 31
- Fig. 3.2.** The XRD patterns of different Cu contents NiCu/ γ - Al_2O_3 . 32
- Fig. 3.3.** The XRD patterns of different Cu contents NiCu/ γ - Al_2O_3 (reduced and spent) catalysts. 33
- Fig. 3.4.** The XPS spectra of different Cu contents NiCu/ γ - Al_2O_3 (fresh) catalyst: (a) Ni 2p spectra, (b) Cu 2p spectra. 34
- Fig. 3.5.** Different bimetal effects for NiM/ γ - Al_2O_3 catalytic activity test (the reaction conditions: T=350 °C, P=1.0 MPa, TOS=3 h, LHSV=1 h⁻¹). 35
- Fig. 3.6.** Temperature effects for NiCu/ γ - Al_2O_3 catalytic activity test (the reaction conditions: P=1.0 MPa, TOS=3 h, LHSV=1 h⁻¹). 36
- Fig. 3.7.** Pressure effects for NiCu/ γ - Al_2O_3 catalytic activity test (the reaction conditions: T=350 °C (a), T=300 °C (b), TOS=3 h, LHSV=1 h⁻¹). 46
- Fig. 3.8.** LHSV effects for NiCu/ γ - Al_2O_3 catalytic activity test (the reaction conditions: T=350 °C, P=1.0 MPa, TOS=3 h). 47

reaction conditions: P=30 bar (a), P=80 bar (b), T=350 °C,
TOS=3 h). 48

Fig. 3.9. Cu contents effect for NiCu/ γ -Al₂O₃ catalytic activity test
(the reaction conditions: T=350 °C, P=30 bar, TOS=3 h,
LHSV= 1 h⁻¹). 50

Fig. 3.10. Longevity catalytic activity test by Ni(18.1)Cu(4.9)/ γ -
Al₂O₃ (the reaction conditions: T=350 °C, P=30 bar,
LHSV=1 h⁻¹). 52



1. INTRODUCTION

1.1. Research background

Non-edible vegetable oil from biomass-derived feedstocks can be considered as a promising alternative energy source to replace the limited fossil fuels used for power generation. There are many benefits of bio-fuels; they are renewable, sustainable, offer clean combustion, improved rural economies and increased energy security [1-3]. Owing to the significant use levels and lower prices as compared to edible oils, the production of bio-fuels from non-edible oils would be an effective means of overcoming the associated issues with edible oils [4]. However, the potential for transferring non-edible types of oil into bio-fuels should be carefully examined, as the physical and chemical properties of bio-fuels produced from non-edible oils must satisfy certain criteria.

All commercial fuels have physicochemical-related criteria. As the Korean government has utilized a renewable portfolio standard (RPS)

since 2012, producers have been seeking and using a wide range of sustainable sources to meet the RPS quota. One of these efforts, a power bio-fuel oil demonstration project, is underway to assess the operability and compatibility with fossil fuels. It has been operated from 2014 [5]. The bio-fuel is a mixture of vegetable oil and animal fats or associated fatty acid esters. These should meet certain specification [Table 1.1, 발전용 바이오중유 시범보급 사업 추진에 관한 고시(산업부고시 2014-1 호)] before they can be used for power generation [6, 7].

The iodine value (IV) is used for the characterization of bio-fuels to assess the extent of unsaturation considering the existence of unsaturated long-chain fatty acids and/or their derivative compounds. The higher the IV, the more C=C bonds are present. The existence of unsaturated compounds could lead to undesirable polymerization or other reactions during storage, which could decrease the fuel quality [8]. Another important quality measurement of bio-fuels is the total acid number (TAN). The higher the TAN, the more acidity is present, increasing the

corrosion risk to machinery and storage tanks [9]. Hydrogenation is an attractive upgrading technology which serves to enhance the product properties of vegetable oil. At present, non-sulfided Ni-based bimetallic catalysts containing NiZn/Al₂O₃ and NiFe/Al₂O₃ have attracted more interest owing to their excellent catalytic activities and stability levels with regard to upgrading vegetable oil or bio oil [10, 11].

In this study, non-edible vegetable oil hydrogenation over NiM/γ-Al₂O₃ bimetallic catalysts was investigated to assess the effects of the bimetal and reaction conditions. To evaluate the extent of upgraded oils, the iodine value and the total acid number were analyzed. γ-Al₂O₃ supported NiM/γ-Al₂O₃ (M₁=Zn, Fe, Cu and Co, 15 wt% Ni, Ni/M₁ molar ratio=2/1; M₂=Pd and Pt, 15 wt% Ni, Ni/M₂ molar ratio=20/1) bimetallic catalysts were prepared by a co-impregnation method and characterized by BET, XRF, XRD and XPS. Screening bimetal effect activity tests were conducted under the condition of 350 °C, 30 bar and LHSV=1 h⁻¹ in a packed-bed reactor, followed by a reaction condition

effect activity test under a range of temperatures (250-400 °C), pressures (5-80 bar) and LHSVs (1-10 h⁻¹). In addition, the influence of the bimetal content (0-23 wt% in the catalyst) was assessed, and a longevity test was also conducted. A 1/1 (v/v %) mixture of cashew nut shell liquid (CNSL) and palm acid oil (PAO) was selected as the feed (IV:186.30, TAN:42.90).



Table 1.1. The quality standards of bio-fuel for power generation

Properties	Units	Test method	Spec.	
Flashpoint	°C	KS M ISO 2719	70	
Kinematic viscosity (50 °C)	mm ² /s	KS M ISO 3104	20-100	
Carbon residue	wt %	KS M ISO 10370	Max. 10	
Sulfur	wt %	KS M ISO 8754	Max. 0.10	
Ash	wt %	KS M ISO 6245	Max. 0.10	
Copper strip corrosion (50 °C, 3h)	-	KS M ISO 2160	Max. 1 b	
Pour point	°C	KS M ISO 3016	Max. 27.5	
Density (15 °C)	kg/cm ³	KS M ISO 12185	Max. 991	
Water	wt %	KS M 0010	Max. 0.20	
Total acid number	mg KOH/g	KS M ISO 6618	Max. 25	
Alkali metal	Na	mg/kg	AAS	Max. 70
	Ca	mg/kg	AAS	Max. 30
	K	mg/kg	AAS	Max. 70
Iodine value	g/100g	EN 14111	Max. 120	
Nitrogen	wt %	KS M 2112	Max. 0.3	
Vanadium	mg/kg	ICP	Max. 50	
Cross heating values	kcal/kg	KS M 2057	Min. 9000	
Net heating values	kcal/kg	KS M 2057	-	
Water and sediment	vol %	KS M ISO 9030	Max. 0.5	
Si+Al+Fe	mg/kg	ICP	Max. 200	
Phosphorus content	mg/kg	ICP	Max. 100	

1.2. Literature review

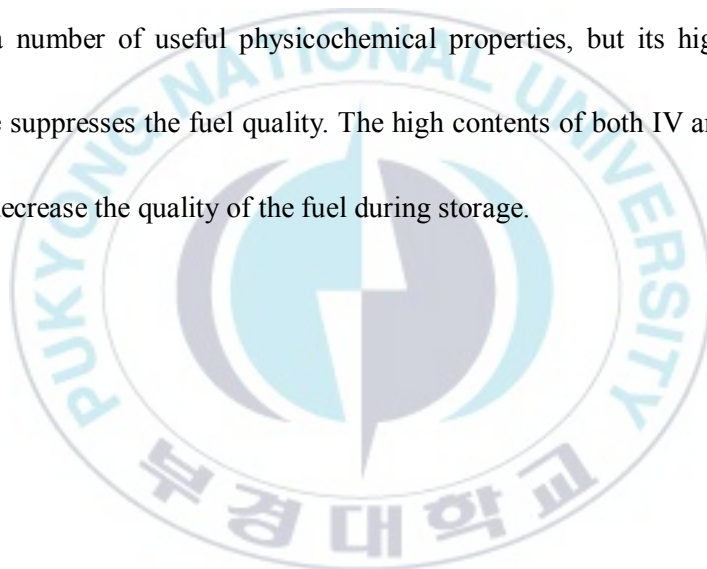
1.2.1. Feedstocks: CNSL and PAO

Cashew Nut Shell Liquid (CNSL) is a common by-product of the cashew industry. The cashew nut has a shell which is approximately one eighth of an inch thick, inside with a soft honey-comb structure containing a dark reddish brown viscous liquid [12]. This is known as CNSL, which is the pericarp fluid of the cashew nut. As shown in Fig. 1.1, it typically contains anacardic acid (60-65%), cardol (15-20%), cardanol (10%), and traces of 2-methyl cardanol [13]. In addition, CNSL is often considered as an inexpensive and better materials for unsaturated phenol [14].

Palm Acid Oil (PAO) is a bio-fuel feedstock derived from palm oil mill effluent (POME). PAO is a by-product of the chemical refining of palm oil and consists of free fatty acids (FFA, over 50%), neutral oil, moisture (2-3%), and other impurities (Table 1.2). It is closely related to

palm fatty acid distillate (PFAD), but its FFA is generally lower. PAO is increasingly used in mixes in bio-fuel transportation fuel [15].

Table 1.3 shows the physical and chemical characteristics of CNSL and PAO. The CNSL samples meet most of the specifications for bio-fuel oil for power generation, apart from its high IV. In contrast, PAO has a number of useful physicochemical properties, but its high TAN value suppresses the fuel quality. The high contents of both IV and TAN can decrease the quality of the fuel during storage.



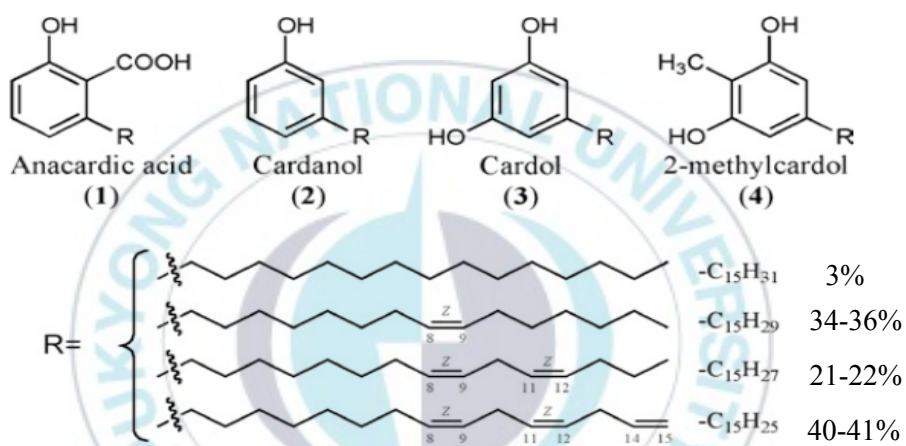


Fig. 1.1. The structures of CNSL constituents.

Table 1.2. The Compositions of FFA in PAO

FFA chain lengths	Name	Composition
C14:0	Myristic acid (saturated)	1.0%
C16:0	Palmitic acid (saturated)	43.5%
C18:0	Stearic acid (saturated)	4.3%
C18:1	Oleic acid (monounsaturated)	36.6%
C18:2	Linoleic acid (polyunsaturated)	9.1%
	Other/Unknown	5.5%

Table 1.3. The physicochemical characteristics of CNSL and PAO

Properties	Units	Spec.	CNSL ^a	PAO ^b
Flashpoint	°C	70	214	-
Kinematic viscosity (50 °C)	mm ² /s	20-100	54.20	-
Carbon residue	wt %	Max. 10	2.01	-
Sulfur	wt %	Max. 0.10	0.02	-
Ash	wt %	Max. 0.10	0.05	0.01
Copper strip corrosion (50 °C, 3h)	-	Max. 1 b	1 a	-
Pour point	°C	Max. 27.5	-42.0	-
Density (15 °C)	kg/cm ³	Max. 991	955	918
Water	wt %	Max. 0.20	0.08	0.03
Total acid number	mg KOH/g	Max. 25	9.5	117.5
Alkali metal	Na	mg/kg	15.2	-
	Ca	mg/kg	13.6	-
	K	mg/kg	57.7	-
Iodine value	g/100g	Max. 120	259	78.9
Nitrogen	wt %	Max. 0.3	0.13	-
Vanadium	mg/kg	Max. 50	< 1	-
Cross heating values	kcal/kg	Min. 9000	9690	-
Net heating values	kcal/kg	-	9084.7	-
Water and sediment	vol %	Max. 0.5	0.45	-
Si+Al+Fe	mg/kg	Max. 200	109.7	-
Phosphorus content	mg/kg	Max. 100	6.2	-

^a: Analysis by Korea Adjusters and Surveyors Corporation

^b: Analysis by CS Energy Co., LTD, Korea.

1.2.2. Hydrogenation

Hydrogenation is an attractive upgrading technology to enhance the product properties of vegetable oil or bio oil [16]. Many researchers pointed out that the hydrogenation of vegetable oil is more favorable and it can be combined with existing crude oil refineries because it is similar to the upgrading of petroleum [17].

Hydrogenation consists of various catalytic reaction mechanisms in the presence of hydrogen. The double bonds present in the oil are saturated through the catalytic addition of hydrogen at certain temperatures and pressures in a reactor. Hydrogenation removes the oxygen of triglycerides, esters and free acids molecules by hydrodeoxygenation (HDO), decarbonylation and decarboxylation reactions to yield mainly n-alkanes. Meanwhile, depending on the characteristics of the bimetallic catalysts, the cracking and hydrocracking of hydrocarbon chains could also be significant, and these reactions help to improve the quality of the fuel [18]. Furthermore,

hydrodesulfurization (HDS) and hydrodenitrogenation (HDN) reactions can occur simultaneously [19].

1.2.3. Catalysts

Catalysts play important roles in the hydrogenation process. Many types of catalysts have been studied with different active phases, promoters and supports for the hydrogenation of vegetable oil or bio oil.

For instance, noble metal monometallic catalysts (Pd, Pt, Rh and Ru) on various supports (Al_2O_3 , SiO_2 , TiO_2 , ZrO_2 and CeO_2) have been used extensively [20-22]. These catalysts showed good hydrogenation, HDO, HDS and HDN activity for compounds with a wide variety of functional groups. However, scarcity and high cost of noble metals make them useless for industrial applications.

Transition metal supported catalysts (Ni, Mo, Co, Fe, Cu) have been investigated because of their low cost and good catalytic performances [23-25]. Traditional HDS catalysts such as sulfided $\text{NiMo}/\text{Al}_2\text{O}_3$, $\text{NiMo}/\text{Al}_2\text{O}_3\text{-SiO}_2$ and $\text{CoMo}/\text{Al}_2\text{O}_3$ were also reported for

hydrogenation of vegetable oil [26-28]. However, the sulfided catalysts result in the problem of sulfur usage and product contamination.

In recent studies, the addition of bimetals to transition-metal catalysts has been reported, as changes in electronic structures and/or the surface ensemble size due to the presence of adjacent atoms may enhance the catalyst activity and stability. Moreover, bimetallic NiZn [10] and NiFe [11] catalysts have been also investigated, showing good catalytic performance for the hydrogenation of certain model compounds, such as phenol, anisole, and guaiacol.

1.3. Objectives

The aim of our study is to present NiM/ γ -Al₂O₃, especially NiCu/ γ -Al₂O₃ bimetallic catalyst could improve the catalytic activities and stabilities of upgrading of non-edible vegetable oil. And the best reaction condition was also identified. Non-edible vegetable oil such as CNSL and PAO is potential for bio-fuels used in power generation that can replace current dependence on the fossil fuels resources worldwide.

2. MATERIALS AND EXPERIMENTAL

2.1. Materials

The feedstocks of Cashew Nut Shell Liquid (CNSL) and Palm Acid Oil (PAO) were collected from CS Energy company (Busan, Korea). The support used in this study was γ -Al₂O₃ (Thermo Fisher, γ -phase). The chemicals used for the synthesis of the catalyst were Ni(NO₃)₂•6H₂O (Samchun, 98.0%), Zn(NO₃)₂•6H₂O (Junsei, 96.0%), Fe(NO₃)₂•9H₂O (Katayama, 99.0%), Cu(NO₃)₂•3H₂O (Junsei, 99.0%), Co(NO₃)₂•6H₂O (Junsei, 97.0%), Pd(NO₃)₂•2H₂O (Kojima, 99.0%) and Pt(NH₃)₄(NO₃)₂ (Aldrich, 50wt% Pt). The gases were utilized in the catalytic activity test were H₂ (PSG GO., LTD, 99.999%), N₂ (Daesung Industrial Gases GO., LTD, 99.999%).

2.2. Catalyst preparation

γ -Al₂O₃ supported NiM (M₁=Zn, Fe, Cu and Co, 15 wt% Ni, Ni/M₁ molar ratio=2/1; M₂=Pd and Pt, 15 wt% Ni, Ni/M₂ molar ratio=20/1)

bimetallic catalysts were synthesized by the procedure shown in Fig. 2.1 using a co-impregnation method. The γ -Al₂O₃ support was sieved by a mesh with openings ranging from 18 to 40 nm. In order to investigate the Cu effect in the NiCu/ γ -Al₂O₃ bimetallic catalyst, different contents of Cu were applied with a fixed metal loading of 23 wt% and were denoted as Ni(wt%)Cu(wt%)/ γ -Al₂O₃: Ni(23.0)/ γ -Al₂O₃, Ni(20.5)Cu(2.5)/ γ -Al₂O₃, Ni(18.1)Cu(4.9)/ γ -Al₂O₃, Ni(15.0)Cu(8.0)/ γ -Al₂O₃, Ni(11.0)Cu(12.0)/ γ -Al₂O₃, Ni(4.3)Cu(18.7)/ γ -Al₂O₃ and Cu(23.0)/ γ -Al₂O₃.

In the bimetallic catalyst synthesis procedure, the required quantities of Ni(NO₃)₂•6H₂O and bimetal salt were dissolved in 250 mL of deionized water. Followed by adding the γ -Al₂O₃ support into the nickel-bimetal solution and kept for 120 min under stirring. In order to remove water, the mixture was heated and evacuated for 4 hours by means of a rotary evaporator (Eyela, N-1110S-W). After evaporation, the collected wet powder was further dried in an oven at 120 °C for overnight. The powder sample was calcined in the atmosphere at 500 °C

for six hours with the ramping rate of 5 °C/min. All of the catalysts were reduced by H₂ at 550 °C for four hours under a flowrate of 180 mL/min before the catalytic activity test.



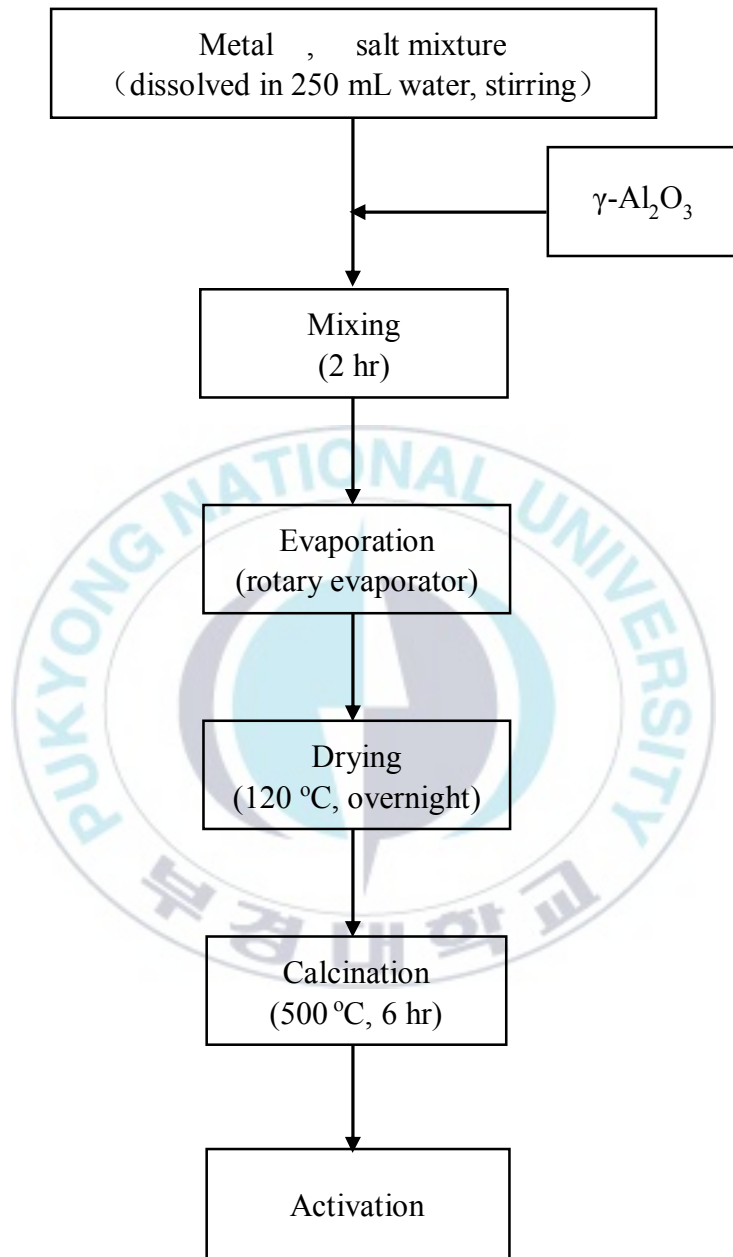


Fig. 2.1. The preparation procedure of bimetallic catalysts.

2.3. Catalyst characterization

2.3.1. Brunauer-Emmett-Teller (BET)

The specific surface area, total pore volume and average pore size were measured at 77.3 K using a static N₂ physisorption method by a Micromeritics' TriStar II 3020 analyzer. The specific surface area of the catalysts was calculated from the adsorption branch of the isotherm and the average pore size was determined using the BJH (Barret-Joyner-Halenda) method. The total pore volume of the catalysts depended on the volume of the adsorbed N₂ at a relative pressure of approximately 0.99.

2.3.2. X-ray fluorescence (XRF)

The actual relationships between the Ni and the bimetal were determined through XRF using a wavelength-dispersive FluoroMate FS-2 (SCINCO, Korea) spectrometer with a primary xenon X-ray source.

2.3.3. X-ray diffraction (XRD)

Powder XRD patterns of fresh, reduced and spent bimetallic catalysts were obtained with an X-ray diffractometer (Rigaku, D/MAX 2500) equipped with Cu K α radiation (40 kV and 100 mA) while scanning at 2 θ from 10° to 90°. The obtained diffraction patterns were identified and compared with reference patterns in the JCPDS (Joint Committee on Powder Diffraction Standards) database. The crystallite size of Ni or M_xO_y on the catalyst was calculated by the Scherrer equation:

$$d = \frac{K\lambda}{\beta \cos\theta} \quad (2.1)$$

Where K is a constant (0.89), λ is the X-ray wavelength (0.154056 nm), and β is the angular full width at half maximum (FWHM) expressed in terms of radians.

2.3.4. X-ray photoelectron spectroscopy (XPS)

X-ray photoelectron spectroscopy (XPS) was used to study the electronic state of the elements that exist within the material. Spectra

were collected using a Thermo VG Scientific MultiLab 2000 spectrometer and a multi-channel detector with nonmonochromatic Al K α radiation, which can endure the high photonic energy levels ranging from 0.1 to 3 keV. The carbonaceous C 1s line (284.6 eV) was used as a reference to calibrate the binding energies.

2.4. Catalytic upgrading

The catalytic activity test of the bimetallic catalyst for vegetable-oil upgrading was conducted using the hydrogenation process, which in this case was performed in a bench-scale packed-bed reactor (Catacube, RTI Engineering Co., Ltd.) with a concurrent downflow of vegetable-oil and hydrogen (Fig. 2.2). The reactor was equipped with a system that controlled the temperature and pressure. Hydrogen was flowed into the CATAcube device using a mass flow controller (Brooks) from a gas cylinder manifold system, and the liquid feed was fed into the reactor using a High Performance Liquid Chromatography pump (Shimadzu).

Before the reaction, the fresh bimetallic catalysts (5 g, 18-40 mesh)

was reduced directly in the reactor under a flow of 99.9999% H₂ (180 mL/min) for four hours at 550 °C under atmospheric pressure. The reaction conditions were as temperature range of 250-400 °C, pressure range of 5-80 bar, and a liquid hourly space velocity (LHSV) range of 1-10 h⁻¹.



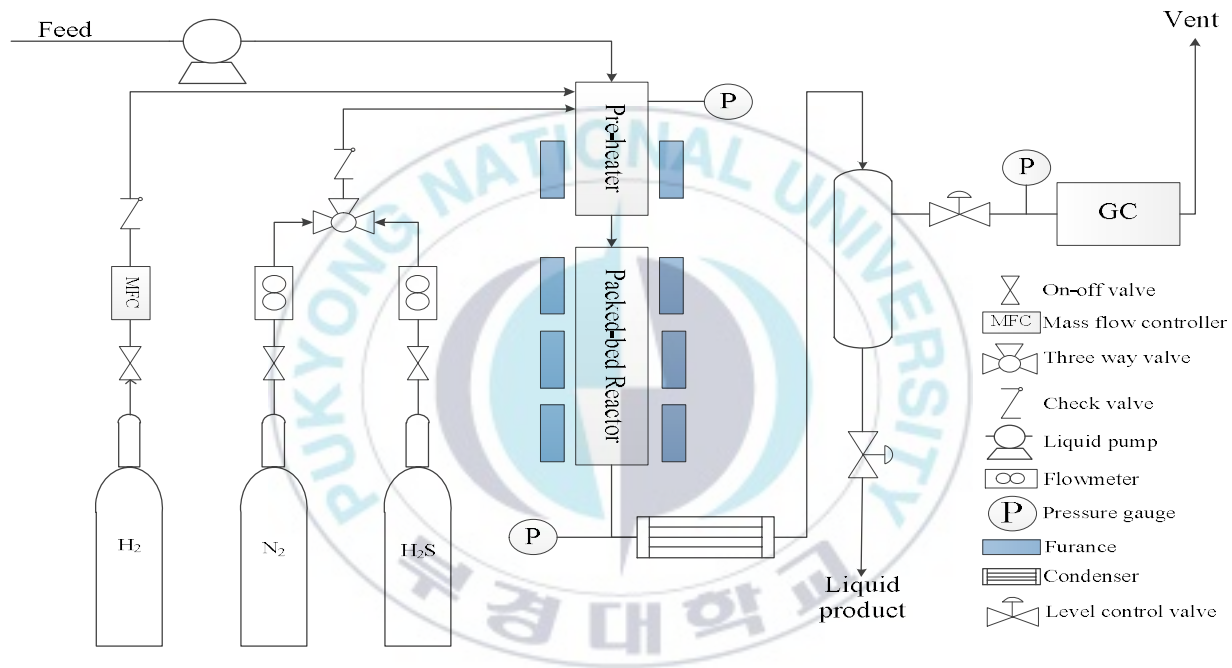


Fig. 2.2. The schematic diagram of packed-bed reactor.

2.5. Analysis of upgraded oil

The iodine value (IV) and total acid number (TAN) were analyzed according to Korean standards KS H ISO 3961 and KS H ISO 6618, respectively. The IV and TAN measurements for each sample were both repeated three times.

IV is the mass of halogen bound to the double-bonds contained in 100 g of oil. According to the KS H ISO 3961 standard, this is expressed in grams of iodine (I_2) per 100 g of oil sample. The mechanism is based on the reaction between an amount of Wijs (ICl) solution and the double-bonds contained in the oil sample. By adding potassium iodide (KI), the excess of the Wijs reagent becomes I_2 . Then, the concentration of the formed I_2 is determined by titration with sodium thiosulfate. The 110–140 mg oil samples were used for the iodine value analysis.

TAN represents the number of milligrams of potassium hydroxide (KOH) used to neutralize the acidic functional groups present in one gram of a sample of oil. It is expressed in milligram KOH per gram of

sample. To analyze the TAN value, 200-250 mg of sample was dissolved in 20 mL of an ethanol-ether (v/v%=1/1) solution. This mixture was then titrated by a 0.1 M KOH-ethanol solution using phenolphthalein as a color indicator.

The removal efficiency rates of IV and TAN were calculated based on the following equations,

$$\eta_{IV} = (I_0 - I/I_0) * 100\% \quad (2.2)$$

$$\eta_{TAN} = (T_0 - T/T_0) * 100\%, \quad (2.3)$$

Where I_0 and I donate the IV in the feed and the product, respectively, and T_0 and T correspondingly denote the TAN values of the feed and the product.

3. RESULTS AND DISCUSSIONS

3.1. Catalyst characterization

3.1.1. Brunauer-Emmett-Teller (BET)

The textural properties of the synthesized bimetallic NiM/ γ -Al₂O₃ catalysts are shown in Table 3.1. The BET surface area and total pore volume of the Ni and/or bimetal loaded onto γ -Al₂O₃ were decreased significantly compared to the γ -Al₂O₃ support. The average pore size of NiM/ γ -Al₂O₃ catalysts was similar to that of the γ -Al₂O₃ support. After the metal-loading steps, some of the micropores and mesopores of the γ -Al₂O₃ support were filled with metal oxides, possibly reducing their textural properties [10]. Similar decreases in the surface area and total pore volume of the metal-loaded γ -Al₂O₃ catalysts were confirmed by Mariam et al. [29]. The average pore radiuses obtained from the pore size distributions of the support and the catalysts were identical in the range of 106-114 Å.

Table 3.1. Textural properties of different synthesized catalysts

Num.	Catalysts (fresh)	Surface area (m ² /g)	Total pore volume (cm ³ /g)	Pore size (Å)
1	γ -Al ₂ O ₃	222.1	0.627	110.5
2	Ni(15.0)Zn(8.3)/ γ -Al ₂ O ₃	141.5	0.398	112.4
3	Ni(15.0)Fe(7.1)/ γ -Al ₂ O ₃	161.4	0.437	108.4
4	Ni(15.0)Cu(8.1)/ γ -Al ₂ O ₃	149.8	0.416	112.6
5	Ni(15.0)Co(7.5)/ γ -Al ₂ O ₃	139.9	0.391	111.8
6	Ni(15.0)Pd(1.4)/ γ -Al ₂ O ₃	168.1	0.453	107.8
7	Ni(15.0)Pt(2.5)/ γ -Al ₂ O ₃	162.7	0.446	109.7
8	Ni(23.0)/ γ -Al ₂ O ₃	153.7	0.402	104.6
9	Ni(20.5)Cu(2.5)/ γ -Al ₂ O ₃	150.2	0.400	106.6
10	Ni(18.1)Cu(4.9)/ γ -Al ₂ O ₃	150.9	0.398	105.6
11	Ni(11.0)Cu(12.0)/ γ -Al ₂ O ₃	150.5	0.406	110.3
12	Ni(4.3)Cu(18.7)/ γ -Al ₂ O ₃	156.2	0.435	113.8
13	Cu(23.0)/ γ -Al ₂ O ₃	159.3	0.455	114.2

3.1.2. X-ray fluorescence (XRF)

The results of XRF analyses of the samples are presented in Table 3.2. The actual atomic ratio of Ni to bimetal in the catalysts was slightly different from the pre-set value. This difference arose due to the slight metal loss during the catalyst synthesis process. In NiCu/ γ -Al₂O₃ catalysts, as the Cu content is increased, the atomic ratio of Cu to Al and the composition of Cu also increase.

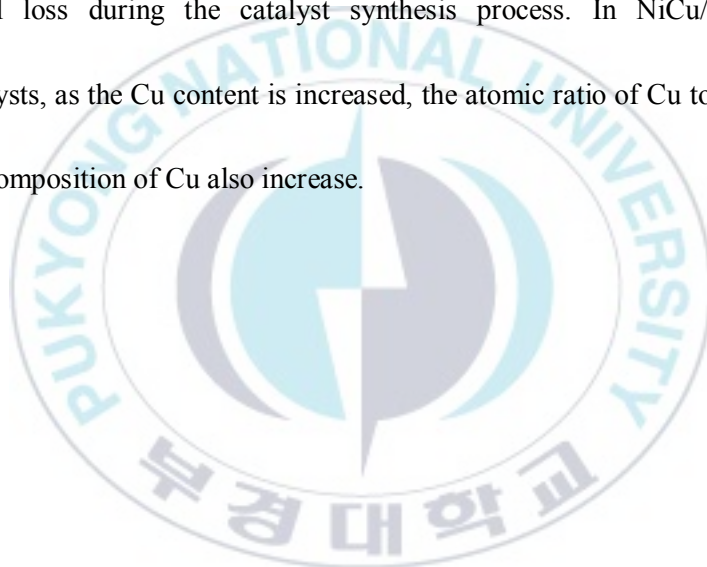


Table 3.2. XRF data of different synthesized catalysts

Num.	Catalysts (fresh)	[Ni]/[M] ^a (theoretical)	[Ni]/[M] (samples)	[Ni]/[Al]	[M]/[Al]	Chemical composition
1	Ni(15.0)Zn(8.3)/ γ -Al ₂ O ₃	2	1.477	0.172	0.116	Ni _{0.60} Zn _{0.40}
2	Ni(15.0)Fe(7.1)/ γ -Al ₂ O ₃	2	3.063	0.228	0.075	Ni _{0.75} Fe _{0.25}
3	Ni(15.0)Cu(8.1)/ γ -Al ₂ O ₃	2	2.016	0.186	0.098	Ni _{0.67} Cu _{0.33}
4	Ni(15.0)Co(7.5)/ γ -Al ₂ O ₃	2	1.626	0.180	0.111	Ni _{0.62} Co _{0.38}
5	Ni(15.0)Pd(1.4)/ γ -Al ₂ O ₃	20	16.225	0.197	0.012	Ni _{0.94} Pd _{0.06}
6	Ni(15.0)Pt(2.5)/ γ -Al ₂ O ₃	20	16.414	0.196	0.012	Ni _{0.94} Pt _{0.06}
7	Ni(23.0)/ γ -Al ₂ O ₃	-	-	0.303	-	-
8	Ni(20.5)Cu(2.5)/ γ -Al ₂ O ₃	9	8.038	0.354	0.044	Ni _{0.89} Cu _{0.11}
9	Ni(18.1)Cu(4.9)/ γ -Al ₂ O ₃	4	3.803	0.312	0.082	Ni _{0.79} Cu _{0.21}
10	Ni(11.0)Cu(12.0)/ γ -Al ₂ O ₃	1	1.041	0.159	0.153	Ni _{0.51} Cu _{0.49}
11	Ni(4.3)Cu(18.7)/ γ -Al ₂ O ₃	0.25	0.291	0.063	0.215	Ni _{0.23} Cu _{0.77}
12	Cu(23.0)/ γ -Al ₂ O ₃	-	-	-	0.242	-

^a: [Ni]/[M] means the atomic ratio.

3.1.3. X-ray diffraction (XRD)

The XRD spectra of the NiM/ γ -Al₂O₃ (M= Zn, Fe, Cu, Co, Pd and Pt) fresh catalysts are shown in Fig. 3.1. Similar diffraction peak positions of the γ -Al₂O₃ structure at 20.57°, 37.20°, 45.92° and 66.79° were determined using JCPDS Card No. 29-0063. The results indicate that the crystalline structure of the γ -Al₂O₃ support remains after Ni and/or bimetal loading [10]. Ni/ γ -Al₂O₃ catalysts showed peaks of the NiO phase at 37.19° (111), 43.22° (200), 62.86° (220), 75.36° (311) and 79.42° (222) according to JCPDS Card No. 78-0643. The NiM/ γ -Al₂O₃ (M= Zn, Fe, Cu and Co) catalysts showed peaks of both NiO and M_xO_y, and the peaks of M_xO_y corresponded to JCPDS Card Nos. 99-0111 (ZnO), 75-0449 (Fe₃O₄), 48-1548 (CuO) and 43-1003 (Co₃O₄). The peak patterns of PdO and PtO₂ were not found among the XRD patterns, possibly because the small amount of noble metal was highly dispersed. Compared to the Ni/ γ -Al₂O₃ catalyst, the decreased intensity of the Ni peaks' in the NiM/ γ -Al₂O₃ catalyst indicates that moderate incorporation

of the bimetal improved the dispersion of nickel.

The XRD spectra of NiCu/ γ -Al₂O₃ fresh catalysts are shown in Fig. 3.2. The Cu/ γ -Al₂O₃ showed the peaks of CuO at 32.50° (110), 35.48° (11-1), 38.64° (111), 48.80° (20-2), 53.37° (020), 58.16° (202), 61.54° (11-3), 68.12° (220), 72.34° (221) and 75.12° (004) were determined using JCPDS Card No. 48-1548. With increasing the amount of Cu (0-23 wt%) resulted in diffraction peaks of NiO broadening and weakening gradually and formed CuO peaks. Meanwhile, the angle of NiO peaks are shifted toward smaller angles compared with monometallic NiM/ γ -Al₂O₃ catalyst.

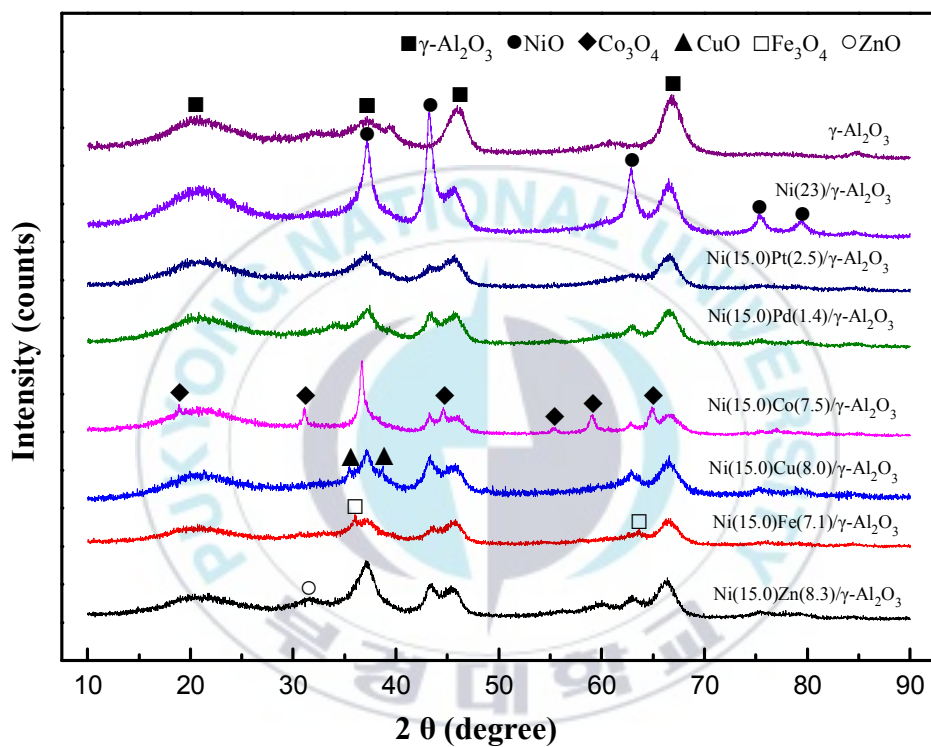


Fig. 3.1. The XRD patterns of different bimetal types for NiM/ $\gamma\text{-Al}_2\text{O}_3$.

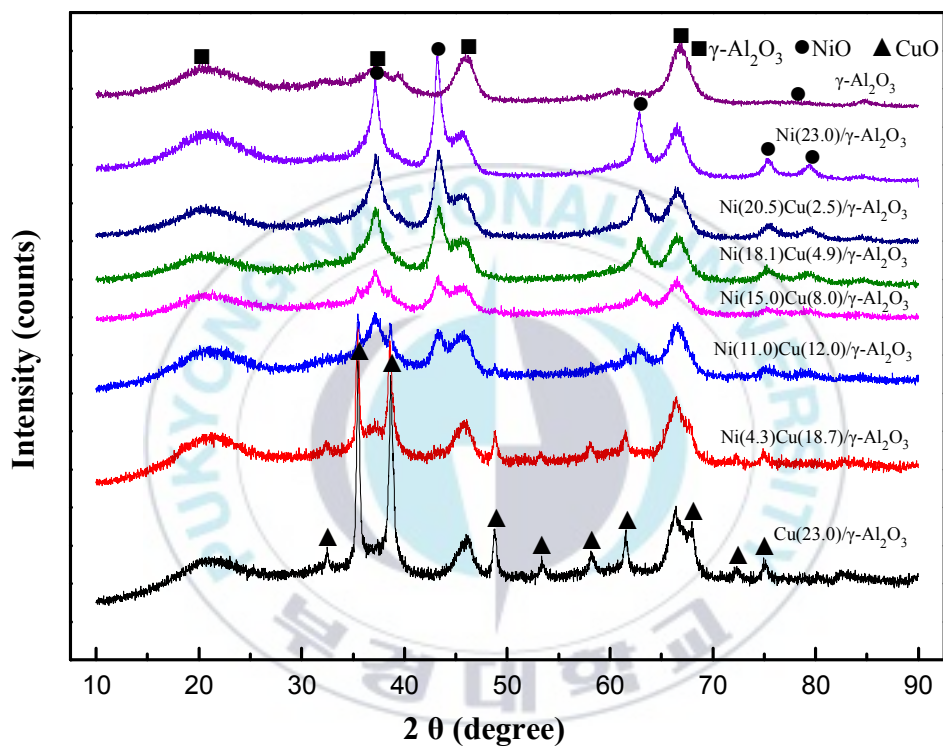


Fig. 3.2. The XRD patterns of different Cu contents NiCu/γ-Al₂O₃ (fresh) catalyst.

The XRD spectra of the reduced NiCu/ γ -Al₂O₃ and the spent catalysts are shown in Fig. 3.3. Both NiO and CuO were fully reduced to metallic Ni and Cu, respectively. In the reduced Ni/ γ -Al₂O₃, similar diffraction peak positions of the Ni structure at 44.46° (111), 51.80° (200), and 76.40° (220) were determined using JCPDS Card No. 04-0850. The reduced Cu/ γ -Al₂O₃ showing peaks of Cu at 43.26° (111), 50.40° (200), 74.06° (220) were determined using JCPDS Card No. 04-0836. With an increase in the amount of Cu (0-23 wt%), the diffraction peaks of Ni broadening were reduced and gradually weakened. Meanwhile, the angle of the Ni peaks shifted to a low degree and became close to those of the Cu peaks, indicating the formation of a NiCu solid solution (or alloy) [30]. The active phase of the catalysts (Ni, Cu or NiCu) remained stable after it was used in the reactions, and there are no diffraction peaks related to the NiO or CuO phases. This outcome indicates good stabilization of the active phase in our synthesized NiCu/ γ -Al₂O₃ catalysts.

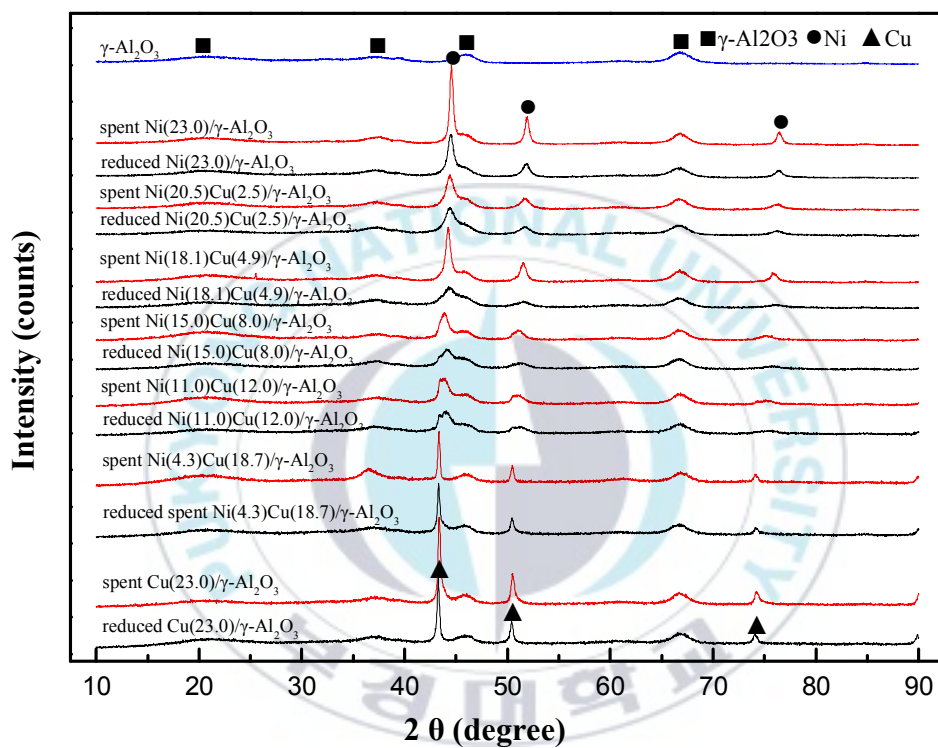


Fig. 3.3. The XRD patterns of different Cu contents NiCu/γ-Al₂O₃ (reduced and spent) catalyst.

The mean crystallite size of the Ni (Cu or NiCu) crystallites in the NiCu/ γ -Al₂O₃ catalyst was calculated by the Scherrer equation using the peak with the highest intensity peak ($2\theta = 43.26$ - 44.46°), which corresponds to the (111) crystal plane. Table 3.3 lists the results obtained from the both reduced and spent catalysts. Concerning the reduced catalysts, the appropriate addition of copper resulted in a reduction of the crystallite size. On the other hand, larger amounts of added copper do not promote an extra reduction in the crystallite sizes, as the formation of Cu leads to large crystallites. Meanwhile, the crystallites of the Ni (Cu or NiCu) spent catalysts were larger than those from the reduced catalyst, showing that the sintering that occurred was insignificant. Moreover, the corresponding crystalline sizes of Ni and Cu were 24.0 nm and 43.8 nm in the monometallic spent catalyst, whereas the crystallite size of the NiCu bimetallic catalyst was much lower. This implies that the addition of copper effectively prevents the nickel particles from sintering during the course of the reaction.

Table 3.3. Crystallite size obtained from reduced and spent NiCu/ γ -Al₂O₃ catalysts

Num.	Catalysts (fresh)	Crystallite size of reduced catalyst ^a (nm)	Crystallite size of spent catalyst (nm)
1	Ni(23.0)/ γ -Al ₂ O ₃	13.0	24.0
2	Ni(20.5)Cu(2.5)/ γ -Al ₂ O ₃	7.3	9.9
3	Ni(18.1)Cu(4.9)/ γ -Al ₂ O ₃	6.6	15.8
4	Ni(15.0)Cu(8.1)/ γ -Al ₂ O ₃	7.2	9.9
5	Ni(11.0)Cu(12.0)/ γ -Al ₂ O ₃	9.5	9.8
6	Ni(4.3)Cu(18.7)/ γ -Al ₂ O ₃	34.4	37.1
7	Cu(23.0)/ γ -Al ₂ O ₃	39.3	43.8

^a: Calculated by the Scherrer equation using the (111) plane of Ni (Cu or NiCu).

3.1.4. X-ray photoelectron spectroscopy (XPS)

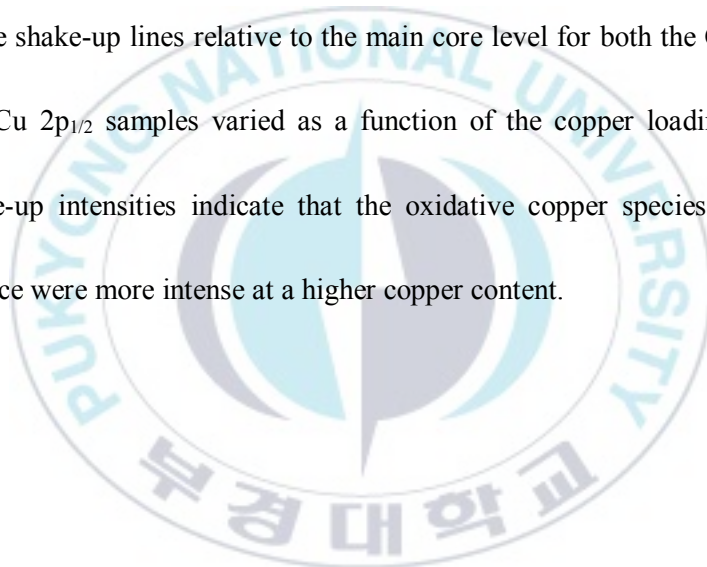
The Ni 2p and Cu 2p spectra of NiCu/ γ -Al₂O₃ (fresh) catalyst are displayed in Fig. 3.4. All XPS peaks were identified according to published references and an on-line database (srdata.nist.gov/xps).

An analysis of the Ni 2p spectra (Fig. 3.4a) indicates that Ni²⁺ exists mainly on the surface and subsurface layers of the NiCu/ γ -Al₂O₃ (fresh) catalyst. The spectra consist of two sharp peaks which correspond to the Ni 2p_{3/2}–Ni 2p_{1/2} spin-orbit doublet and low-intensity satellites; this finding can be linked to energy loss peaks due to Plasmon excitation in the metal [30]. In contrast to those of the NiCu/ γ -Al₂O₃ (fresh) bimetallic catalyst, the binding energy (BE) of the Ni 2p spectra of the Ni/ γ -Al₂O₃ (fresh) was determined to be 855.0 eV (Ni 2p_{3/2}), a typical characteristic of Ni²⁺ [31]. For the NiCu/ γ -Al₂O₃ (fresh) bimetallic catalyst, the main peak of the Ni 2p spectra appeared at a higher BE level. The shift of Ni 2p_{3/2} BE shifted from 0 to 1 eV when the loading levels of Cu were increased from 0 to 23 wt%, indicating changes in the linking

arrangements of the Ni cations within the lattice in the fresh catalyst. [32] Thus, Ni²⁺ ions surrounded by Cu²⁺ ions (through O²⁻ linkage) as second neighbors showed a peak at higher BE than for isolated Ni²⁺ ions surrounded by other Ni²⁺ cations. In addition, the intensities of the shake-up lines relative to the main core level of both the Ni 2p_{3/2} and Ni 2p_{1/2} levels varied as a function of the copper content. Decreased intensity levels of the Ni 2p spectra were observed with the increase in the Cu content, suggesting that the oxidative nickel species on the surface were relatively less intense with an increase in the copper content.

Fig. 3.4b shows the Cu 2p spectra of the NiCu/ γ -Al₂O₃ (fresh) catalyst. Typically, the Cu 2p_{3/2} BE of CuO is between 933.6 and 934.6 eV [30]. Moreover, the Cu 2p spectra of the different Cu²⁺ compounds were characterized by high-intensity shake-up satellites at a higher binding energy by approximately 9 eV relative to that of the main Cu 2p_{3/2} and Cu 2p_{1/2} peaks. Therefore, the shape of the Cu 2p spectra of the

NiCu/ γ -Al₂O₃ (fresh) catalyst under study indicates the copper mainly in the Cu²⁺ state. Compared to the Cu/ γ -Al₂O₃ (fresh) catalyst, a shift within a small range of Cu 2p_{3/2} BE values occurred in the NiCu/ γ -Al₂O₃ (fresh) bimetallic catalyst, most likely due to the changes in the linking arrangements of Cu cations within the lattice. In addition, the intensities of the shake-up lines relative to the main core level for both the Cu 2p_{3/2} and Cu 2p_{1/2} samples varied as a function of the copper loading. The shake-up intensities indicate that the oxidative copper species on the surface were more intense at a higher copper content.



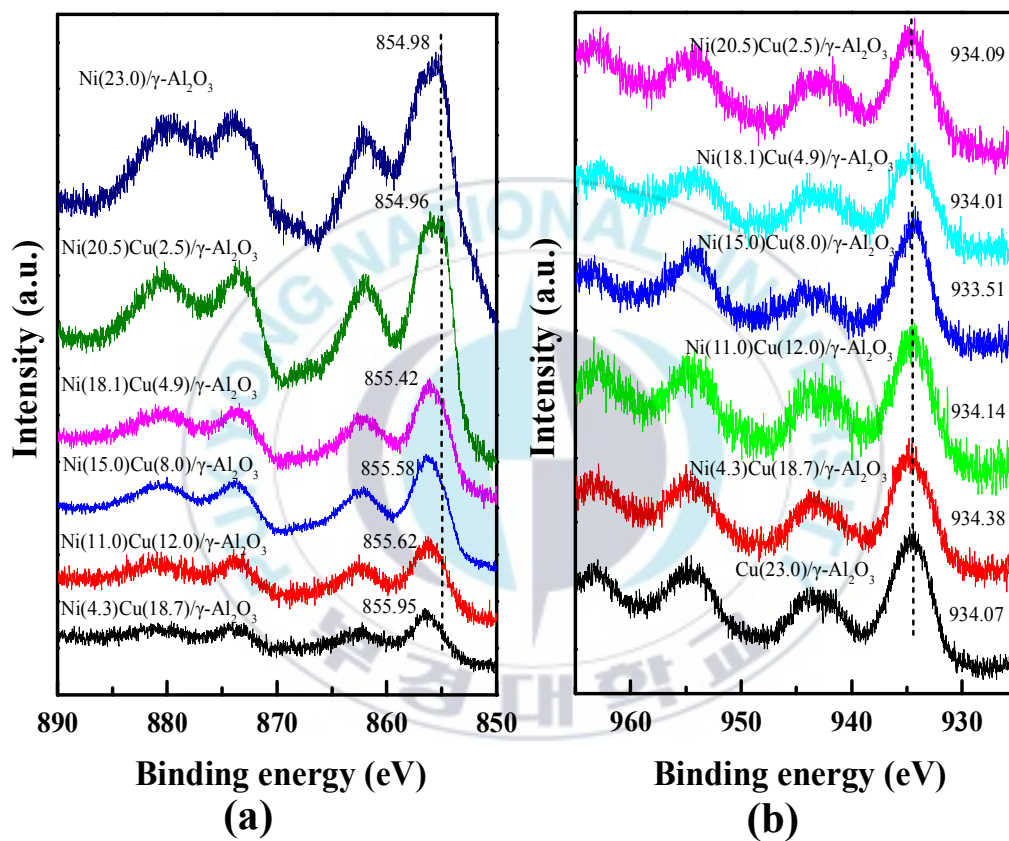


Fig. 3.4. The XPS spectra of different Cu contents NiCu/γ-Al₂O₃ (fresh) catalyst: (a) Ni 2p spectra; (b) Cu 2p spectra.

3.2. Catalytic activity test

3.2.1. Screening test for bimetal effect

We conducted an activity test using various bimetallic NiM/ γ -Al₂O₃ and monometallic Ni/ γ -Al₂O₃ catalysts. The removal efficiency of IV and TAN from upgraded oil is shown in Fig. 3.5. It was found that the addition of different metals resulted in different catalytic performances. With regard to the IV removal efficiency, NiCu/ γ -Al₂O₃, NiPd/ γ -Al₂O₃ and NiPt/ γ -Al₂O₃ all showed significantly higher levels of activity than Ni/ γ -Al₂O₃, whereas Fe and Co suppressed the activity levels. In a test of the TAN removal efficiency, additions of Zn, Cu and Pt to Ni/ γ -Al₂O₃ were found to enhance the catalytic activity dramatically, showing significantly higher activity levels than Ni/ γ -Al₂O₃, while Fe and Co suppressed the activity levels. Particularly, over NiCu/ γ -Al₂O₃ the IV and TAN removal efficiency levels showed considerable improvements of 77.0% and 100.0%, respectively, compared to Ni/ γ -Al₂O₃.

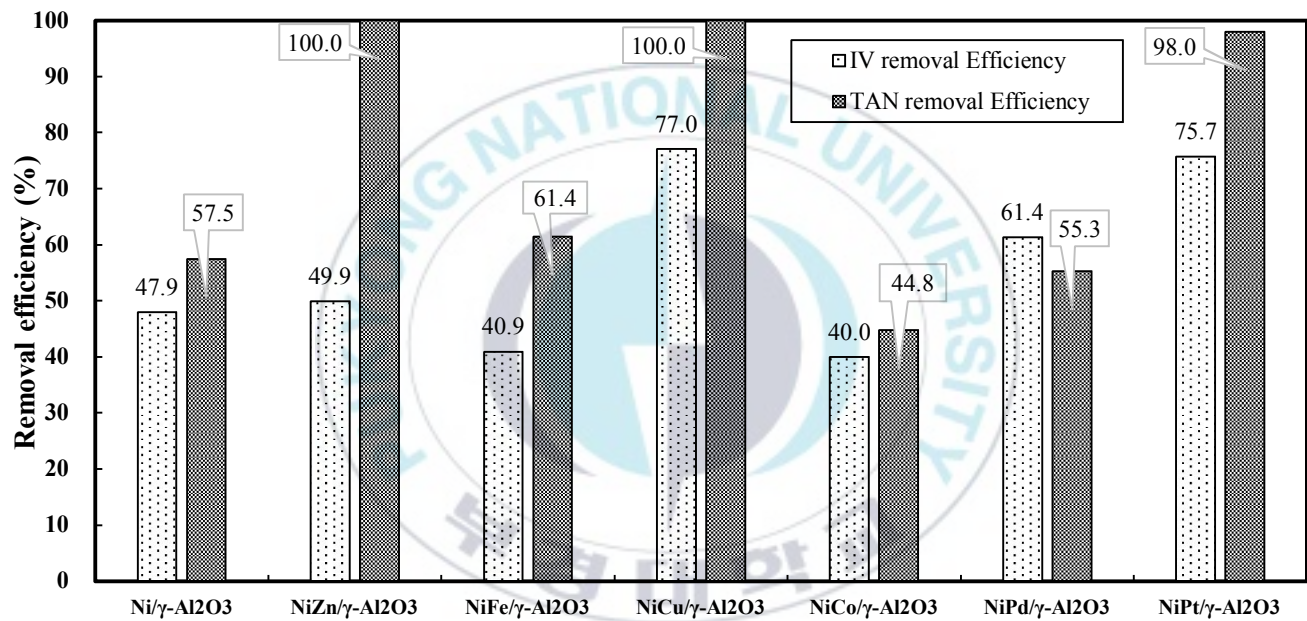


Fig. 3.5. Different bimetal effects for NiM/ γ -Al₂O₃ catalytic activity test (the reaction conditions: T=350 °C, Time on stream (TOS)=3 h, P=30 bar, LHSV=1 h⁻¹).

3.2.2. NiCu/ γ -Al₂O₃: reaction condition effect

3.2.2.1. NiCu/ γ -Al₂O₃: temperature effect

The effects of the temperature on NiCu/ γ -Al₂O₃ performance outcomes were assessed under the following conditions: TOS=3 h, P=30 bar, and LHSV=1 h⁻¹. As shown in Fig. 3.6, the reaction temperature had a significant influence on the NiCu/ γ -Al₂O₃ catalytic activity. Both the IV and TAN removal efficiency rates were highest at 350 °C, indicating that a temperature of 350 °C was favorable for the reaction. Upon an increase in the temperature from 250 °C to 350 °C, the IV and TAN removal efficiency rates increased from 48.4% to 77.0% and from 52.8% to 100.0%, respectively. On the other hand, a reaction temperature of 400 °C suppressed the activities, likely due to the formation of coke. As a result, the hydrogenation of non-edible vegetable oil at 350 °C was selected for further investigation.

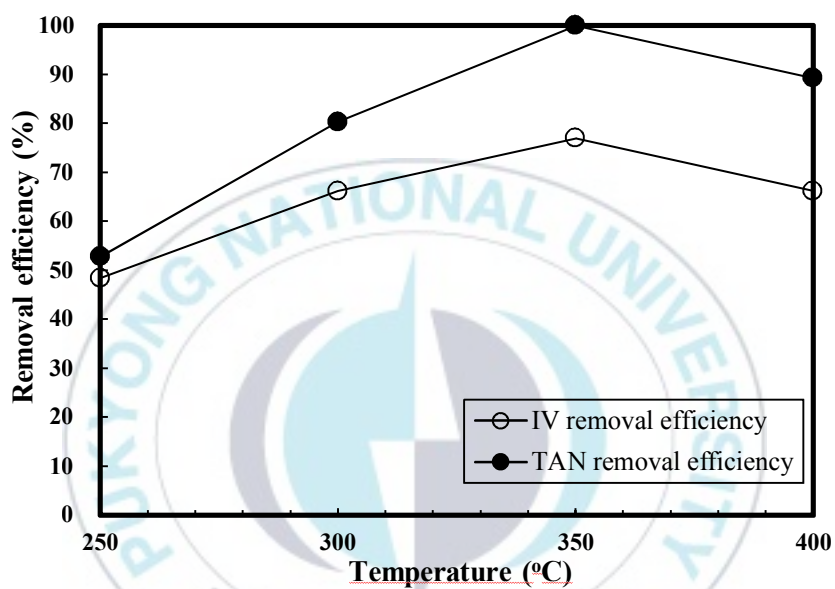
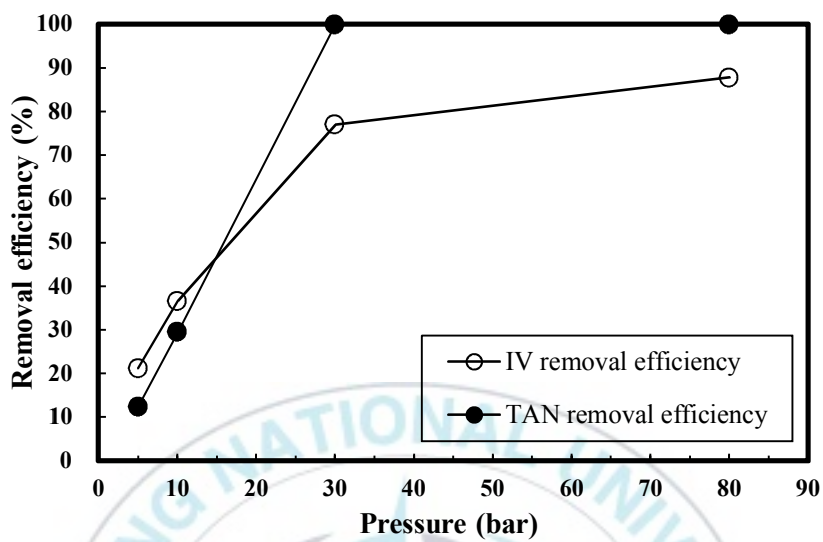


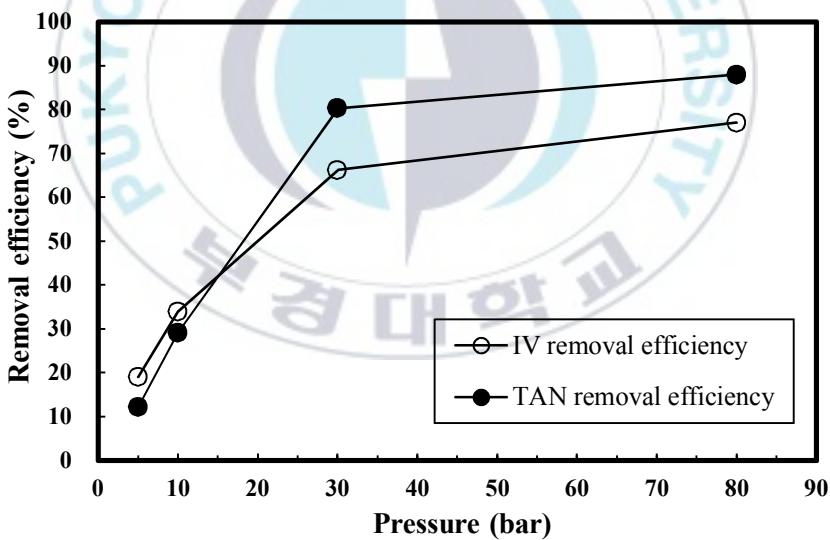
Fig. 3.6. Temperature effects for NiCu/ γ -Al₂O₃ catalytic activity test (the reaction conditions: TOS=3 h, P=30 bar, LHSV=1 h⁻¹).

3.2.2.2. NiCu/ γ -Al₂O₃: pressure effect

As shown in Fig. 3.7, the reaction pressure effect was investigated at two temperatures. Under both 300 °C and 350 °C, the IV and TAN removal efficiency rates showed a similar trend, with only the pressure having a major influence during this test. At 350 °C, when the pressure was increased from 5 bar to 80 bar, the IV and TAN removal efficiency rates increased from 21.2% to 87.8% and from 12.5% to 100.0%, respectively. Increasing the pressure thus enhances the catalytic activity, which may be linked to the enhanced solubility of hydrogen and greater amounts of high hydrogen available during the reaction. In addition, the removal efficiency was increased in a small range when the pressure exceeded 30 bar. As a result, pressure of 30 bar was selected for further investigation.



(a)



(b)

Fig. 3.7. Pressure effects for NiCu/ γ -Al₂O₃ catalytic activity test (the reaction conditions: T=350 °C (a), T=300 °C (b), TOS=3 h, LHSV=1 h⁻¹).

3.2.2.3. NiCu/ γ -Al₂O₃: LHSV effect

Fig. 3.8 shows the effect of LHSV on available catalyst performance at two pressure levels. Under both 30 bar and 80 bar, the IV and TAN removal efficiency showed a similar trend, with only LHSV having significant effects during this test. When the LHSV was increased from 1 to 10 h⁻¹, the IV and TAN removal efficiency rates decreased significantly, providing evidence that the LHSV also had a considerable influence on the performance of the catalytic. As a result, the LHSV at 1 h⁻¹ was selected for further investigation.

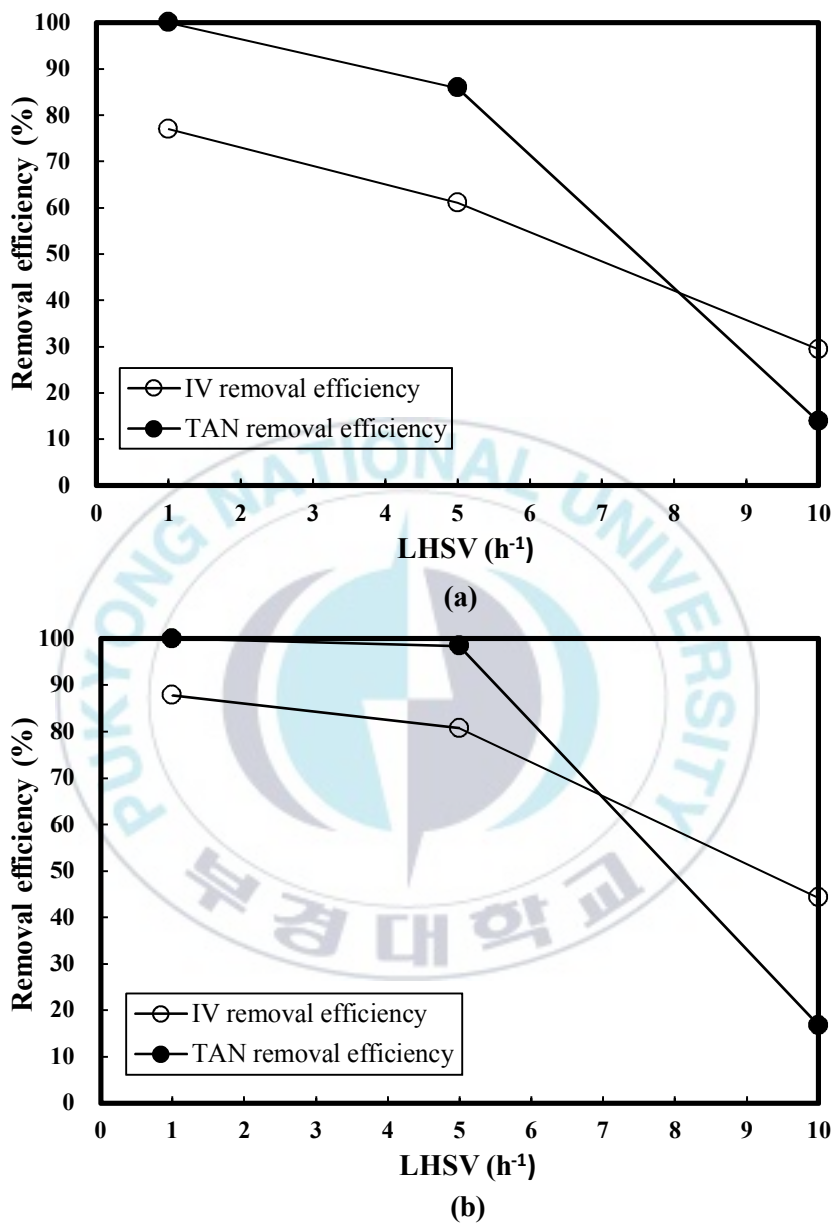


Fig. 3.8. LHSV effects for NiCu/γ-Al₂O₃ catalytic activity test (the reaction conditions: P=30 bar (a), P=80 bar (b), T=350 °C, TOS=3 h).

3.2.2.4. NiCu/ γ -Al₂O₃: Cu contents effect

As shown in Fig. 3.9, the Cu contents had a significant influence on the NiCu/ γ -Al₂O₃ catalytic activity test. As the Cu contents was increased from 0 wt% to 4.9 wt%, both the IV and TAN removal efficiency rates increased, but further increases will have inhibitory effects. This indicates that a moderate Cu addition could greatly improve the catalytic activity compared to the outcome when the monometallic Ni/ γ -Al₂O₃ and Cu/ γ -Al₂O₃ catalysts are used. It showed the synergistic effect of nickel and copper was significant. Over the Ni(18.1)Cu(4.9)/ γ -Al₂O₃ catalyst, the IV and TAN removal efficiency rates reached 81.5% and 100.0%, respectively.

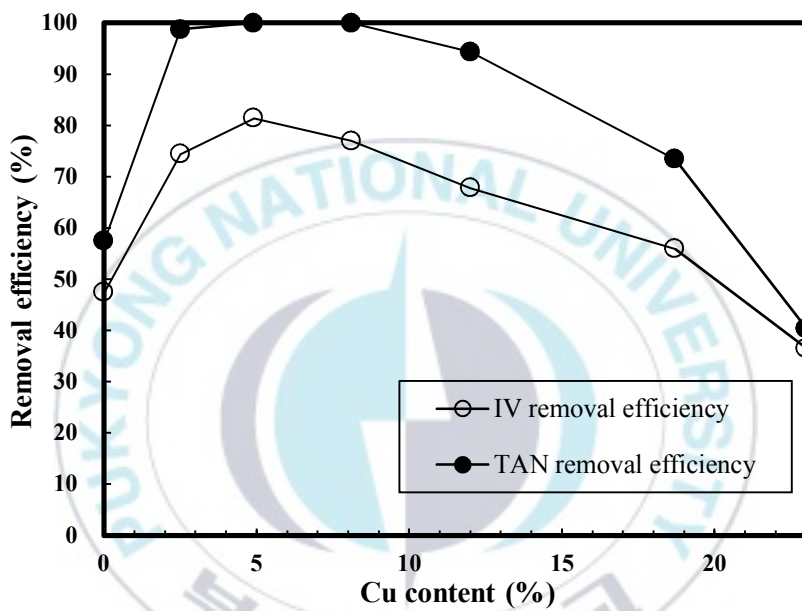


Fig. 3.9. Cu contents effect for NiCu/ γ -Al₂O₃ catalytic activity test (the reaction conditions: T=350 °C, P=30 bar, TOS=3 h, LHSV= 1 h⁻¹).

3.2.3. Longevity test

To gain a better understanding of the catalyst stability, a prolonged evaluation with 60 h on-stream evaluation was conducted with the Ni(18.1)Cu(4.9)/ γ -Al₂O₃ catalysts under the optimum conditions (T=350 °C, P=30 bar and LHSV=1 h⁻¹). As shown in Fig. 3.10, both the IV and TAN removal efficiency rates remained at a high level during a 15-hour reaction. Subsequently, the IV removal efficiency rate decreased significantly up to 33 hours due to the deactivation of the catalyst. Moreover, the TAN removal efficiency decreased in a narrow range and remained stable after 33 hours. Overall, the synthesized Ni(18.1)Cu(4.9)/ γ -Al₂O₃ catalyst showed high activity within 15 hours, with the IV and TAN removal efficiency rate exceeding 75% and 85%, respectively. The catalytic performance was still significant when the time on stream reached 60 hours.

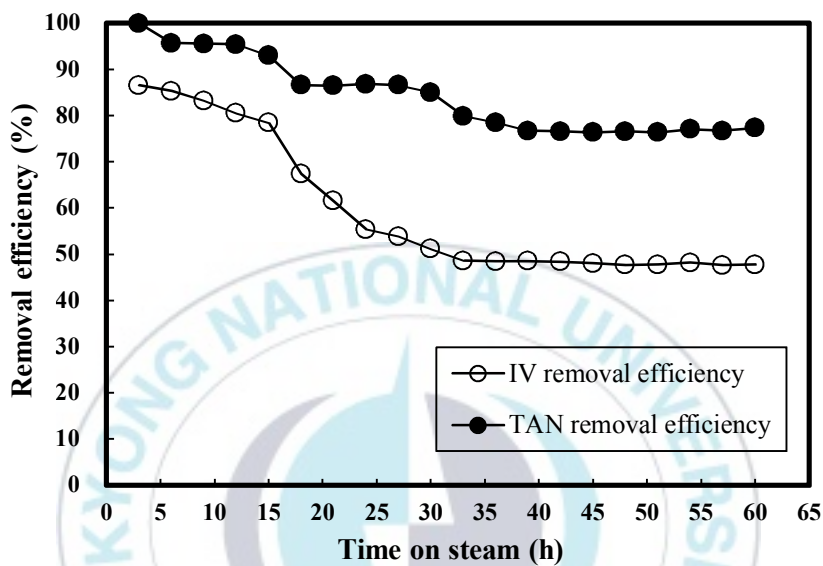


Fig. 3.10. Longevity catalytic activity test by Ni(18.1)Cu(4.9)/ γ -Al₂O₃ (the reaction conditions: T=350 °C, P=30 bar, LHSV=1 h⁻¹).

3.3. Study of catalyst deactivation

Catalyst deactivation is a known problem during the hydrogenation of vegetable oil or bio oil [33, 34]. To investigate the deactivation mechanisms of the catalyst, we measured the compositions of the Ni(18.1)Cu(4.9)/ γ -Al₂O₃ catalyst by ICP-AES (ACTIVA, Horiba JY). As shown in Table 3.4, the Ni, Al and Cu contents of the spent catalyst were respectively 21%, 18% and 23% lower than those of the fresh catalyst, indicating that the activated metal and support run-off may contribute to the deactivation of the catalyst. Moreover, the ICP-AES results showed that the activated metal is poisoned by metals or other heteroatoms carried by the feed. This poisoning by heteroatoms can explain the activity loss [35]. Moreover, the XRD patterns of the reduced and spent catalysts showed that sintering of the activated metal occurred. This is evidence that under the reaction conditions tested here (high pressure, high temperature, and the presence of water), activated metal can agglomerate and become less dispersed.

Table 3.4. ICP-AES data of feedstock and Ni(18.1)Cu(4.9)/ γ -Al₂O₃ catalyst

Num.	Sample	Ni	Al	Cu	Ca	Na	K	Si	Fe	P	Mg
1	CNSL/PAO=1/1	^a N.D	3.7	N.D	12.8	33.8	48.4	6.4	26.5	15.5	N.D
2	NiCu/ γ -Al ₂ O ₃ (fresh)	169093.3	356086.1	49509.3	125.4	241.1	N.D	125.4	48.2	N.D	N.D
3	NiCu/ γ -Al ₂ O ₃ (reduced)	168653.4	364302.2	51130.1	144.1	234.1	N.D	144.1	162.1	N.D	N.D
4	NiCu/ γ -Al ₂ O ₃ (spent)	133177.4	293417.7	38101.6	134.8	431.4	1078.6	287.6	512.3	N.D	N.D

^a: Not detected.

Unit: mg/kg

4. CONCLUSIONS

The bimetallic NiCu/ γ -Al₂O₃ catalyst could greatly enhance the catalytic performance and stability as compared to monometallic Ni/ γ -Al₂O₃ or Cu/ γ -Al₂O₃ catalysts, as the moderate incorporation of Cu promoted the formation of NiCu solid solution (or alloy), which improved the nickel dispersion and prevented the sintering of the metal active sites. Moreover, different reaction condition led to different catalytic activity. With the best catalyst, Ni(18.1)Cu(4.9)/ γ -Al₂O₃, it was demonstrated that the IV and TAN removal efficiency rates could reach 81.5% and 100.0%, respectively, under the conditions of 350 °C, 30 bar, LHSV=1 h⁻¹. According to a longevity test, the catalytic activity remained at a high level for 15 hours, and at 60 hours the activity was still significant. Overall, the unsaturated double-bonds and carboxylic acid in non-edible vegetable oil were decreased significantly by a hydrogenation process over NiCu/ γ -Al₂O₃ bimetallic catalyst.

니켈계 이원금속촉매에 의한 비식용 식물유의 수소화 반응

Hao Zuo

부경대학교 대학원 화학공학과

요약

비식용 식물유는 현재 사용량의 제한성을 지니고 있는 화석 연료를 대체할 수 있는 유망한 에너지원으로 고려되고 있다. 하지만 비식용 식물유의 연료 품질은 화석 연료에 비해 낮고, 높은 산성과 높은 불포화성 때문에 원료 저장 중, 원치않는 산패와 중합반응을 일으키는 단점이 존재한다. 이를 방지하기 위해 촉매를 이용한 수소화 반응은 식물유를 업그레이드하는 유망한 방법으로 현재 NiZn/Al₂O₃ 및 NiFe/Al₂O₃ 과 같은 Ni 기반의 이원금속촉매가 많은 연구자에 의해 관심의 대상이 되고 있다.

본 연구에서는, 식물유의 수소화 반응을 위해 NiM/ γ -Al₂O₃ 이원금속촉매를 테스트하였으며 이원금속 종류, 함량과 반응조건에 대한 효과를 알아보았다. 수소화 반응을 거친 업그레이드된 식물유는 요오드가 (IV) 와 전산가 (TAN) 분석을 통해 반응효율을 평가하였다. γ -Al₂O₃ 를 지지체로 한 NiM/ γ -Al₂O₃ (M₁=Zn, Fe, Cu 및 Co, 15 wt%

Ni, Ni/M₁ molar ratio=2/1; M₂=Pd 및 Pt, 15 wt% Ni, Ni/M₂ molar ratio=20/1) 이원금속촉매는 공침법으로 합성하였으며 BET, XRF, XRD 그리고 XPS 등으로 촉매 특성을 분석하였다. 이들 촉매에 대한 테스트는 충전층반응기에서 350 °C, 30 bar 및 LHSV=1 h⁻¹ 조건에서 수행되었다. 스크리닝 테스트 결과, 가장 유망한 활성을 보인 NiCu/γ-Al₂O₃ 촉매에 대한 반응조건 영향을 알아보기 위해 온도 (250-400 °C), 압력 (5-80 bar) 및 LHSV(1-10 h⁻¹) 를 변화시켜 측정하였다. 또한, NiCu 함량 (0-23wt%)에 따라 산가 및 요오드가 저감 효율을 확인하였으며, 최적의 활성을 갖는 이원금속촉매의 안정성평가도 수행하였다. 반응원료로는 1/1 (v/v%) 의 cashew nut shell liquid (CNSL) 와 palm acid oil (PAO) 혼합물을 사용하였다 (IV:186.30, TAN42.90).

반응활성 결과, 구리와 니켈 성분의 조합에 의한 시너지효과에 의해, NiCu/γ-Al₂O₃ 촉매의 활성이 크게 향상됨을 확인하였다. 반응촉매 중, Ni(18.1)Cu(4.9)/γ-Al₂O₃ (Ni/Cu molar ratio=4/1)이 350 °C, 30 bar, LHSV=1 h⁻¹ 의 조건에서 IV 및 TAN 제거율이 81.5% 및 100.0%로 가장 높게 나타났다. 전반적으로, 비식용 식물유에 포함된 불포화 이중결합과 카르복실산이 NiCu/γ-Al₂O₃ 이원금속촉매로부터 수소화 반응에 의해 현저하게 저감 되었다.

REFERENCES

- [1] Hassan, M. H., Kalam, M. A., An overview of biofuel as a renewable energy source: Development and challenges. *Procedia Engineering* **2013**, *56*, 39-53.
- [2] Khanna, M.; Crago, C. L.; Black, M., Can biofuels be a solution to climate change? The implications of land use change-related emissions for policy. *Interface Focus* **2011**, *1* (2), 233-247.
- [3] Kumar, R.; Rana, B. S.; Verma, D.; Rayaroth, S.; Prasad, V. S.; Sinha, A. K., Hydrotreatment of renewable oils using hierarchical mesoporous H-ZSM-5 synthesized from kaolin clay. *RSC Advances* **2015**, *5* (49), 39342-39349.
- [4] Gashaw, A.; Lakachew, A., Production of biodiesel from non edible oil and its properties. *International Journal of Science, Environment* **2014**, *3* (4), 1544-1562.
- [5] Jang, E. J.; Park, C. K.; Lee, B. H., A study on the storage stability

and malodor of bio-fuel oil. *Transactions of the Korean hydrogen and new energy society* **2017**, 28 (6), 712-720.

[6] Ha, J. H.; Jeon, C. H.; Kwon, Y. C., A study on the emission characteristics for blended power bio-fuel oil. *Transactions of the Korean hydrogen and new energy society* **2015**, 26 (5), 484-492.

[7] Baek, S.; Park, H.; Kim, Y. J.; Kim, T. H.; Kim, H.; Ko, S. H., The demonstration test result of 100% bio heavy oil combustion at the 75 MWE oil fired power plant. *Journal of the Korean Society of Combustion* **2014**, 19 (2), 28-36.

[8] Kumar, R.; Rana, B. S.; Verma, D.; Rayaroth, S.; Prasad, V. S.; Sinha, A. K., Hydrotreatment of renewable oils using hierarchical mesoporous H-ZSM-5 synthesized from kaolin clay. *RSC Advances* **2015**, 5 (49), 39342-39349.

[9] Jiang, Y.; Shi, Y.; Li, Z.; Fan, G., Analysis of the acid value of engine oil based on square wave voltammetry. *Chemical Engineering Transactions* **2016**; 55, 151-156.

- [10] Cheng, S.; Wei, L.; Julson, J.; Muthukumarappan, K.; Kharel, P. R.; Boakye, E., Hydrocarbon bio-oil production from pyrolysis bio-oil using non-sulfide Ni-Zn/Al₂O₃ catalyst. *Fuel Processing Technology* **2017**, *162*, 78-86.
- [11] Yu, X.; Chen, J.; Ren, T., Promotional effect of Fe on performance of Ni/SiO₂ for deoxygenation of methyl laurate as a model compound to hydrocarbons. *RSC Advances* **2014**, *4* (87), 46427-46436.
- [12] Sujaykumar, G.; Ravikumar, R.; Sushilendra, M.; Basavaraj, P., Vinayak, B.; Dhareppa, S.; Santosha, P. V.; Basavaraj, T., Comparative study of waste cooking oil and cashew nut shell oil bio fuel blends with diesel. *Energy and Power* **2017**, *3*, 65-69.
- [13] Rodrigues, F. H. A.; Feitosa, J. P. A.; Ricardo, N. M. P. S.; França, F. C. F. d.; Carioca, J. O. B., Antioxidant activity of cashew nut shell liquid (CNSL) derivatives on the thermal oxidation of synthetic cis-1,4-polyisoprene. *Journal of the Brazilian Chemical Society* **2006**, *17* (2), 265-271.

- [14] Edoga, M.; Fadipe, L.; Edoga, R., Extraction of polyphenols from cashew nut shell. *Leonardo Electronic Journal of Practices and Technologies* **2006**, *5*, 107-112.
- [15] Kuntom, A.; Siew, W. L.; Tan, Y. A., Characterization of palm acid oil. *Journal of the American Oil Chemists' Society* **1994**, *71* (9), 525-528.
- [16] Sonmez, F.; Ercan, H.; Genc, H.; Arslan, M.; Zengin, M.; Kucukislamoglu, M., Hydrogenation of some vegetable oils by scrap automobile catalyst. *Journal of Chemistry* **2013**, *2013*, 1-4.
- [17] Vásquez, M. C.; Silva, E. E.; Castillo, E. F., Hydrotreatment of vegetable oils: A review of the technologies and its developments for jet biofuel production. *Biomass and Bioenergy* **2017**, *105*, 197-206.
- [18] Zacher, A. H.; Olarte, M. V.; Santosa, D. M.; Elliott, D. C.; Jones, S. B., A review and perspective of recent bio-oil hydrotreating research. *Green Chem.* **2014**, *16* (2), 491-515.
- [19] Nagai, M.; Kabe, T., Selectivity of molybdenum catalyst in

hydrodesulfurization, hydrodenitrogenation, and hydrodeoxygenation: effect of additives on dibenzothiophene hydrodesulfurization. *Journal of Catalysis* **1983**, *81* (2), 440-449.

[20] Bhanushali, J. T.; Kainthla, I.; Keri, R. S.; Nagaraja, B. M., Catalytic hydrogenation of benzaldehyde for selective synthesis of benzyl alcohol: A review. *Chemistry Select* **2016**, *1* (13), 3839-3853.

[21] Wilson, K.; Lee, A. F.; Dacquin, J.-P., Heterogeneous catalysts for converting renewable feedstocks to fuels and chemicals. **2012**, *7*, 263-304.

[22] Hollak, S. Catalytic Deoxygenation of fatty acids and triglycerides for production of fuels and chemicals. Utrecht University, **2014**.

[23] Rogers, K. A.; Zheng, Y., Selective deoxygenation of biomass-derived bio-oils within hydrogen-modest environments: A review and new insights. *Chem Sus Chem* **2016**, *9* (14), 1750-1772.

[24] Zhao, X.; Wei, L.; Cheng, S.; Julson, J., Review of heterogeneous catalysts for catalytically upgrading vegetable oils into hydrocarbon

biofuels. *Catalysts* **2017**, 7 (12), 83.

[25] He, Z.; Wang, X., Hydrodeoxygenation of model compounds and catalytic systems for pyrolysis bio-oils upgrading. *Catalysis for Sustainable Energy* **2012**, 1, 28-52.

[26] Gong, S.; Shinozaki, A.; Shi, M.; Qian, E. W., Hydrotreating of Jatropha oil over alumina based catalysts. *Energy & Fuels* **2012**, 26 (4), 2394-2399.

[27] Vlasova, E. N.; Deliy, I. V.; Nuzhdin, A. L.; Aleksandrov, P. V.; Gerasimov, E. Y.; Aleshina, G. I.; Bukhtiyarova, G. A., Catalytic properties of CoMo/Al₂O₃ sulfide catalysts in the hydrorefining of straight-run diesel fraction mixed with rapeseed oil. *Kinetics and Catalysis* **2014**, 55 (4), 481-491.

[28] Baldauf, E.; Sievers, A.; Willner, T., Hydrodeoxygenation of cracked vegetable oil using CoMo/Al₂O₃ and Pt/C catalysts. *International Journal of Energy and Environmental Engineering* **2016**, 7 (3), 273-287.

- [29] Ameen, M.; Azizan, M. T.; Ramli, A.; Yusup, S.; Yasir, M., Physicochemical properties of Ni-Mo/ γ -Al₂O₃ catalysts synthesized via sonochemical method. *Procedia Engineering* **2016**, *148*, 64-71.
- [30] Khromova, S. A.; Smirnov, A. A.; Bulavchenko, O. A.; Saraev, A. A.; Kaichev, V. V.; Reshetnikov, S. I.; Yakovlev, V. A., Anisole hydrodeoxygenation over Ni-Cu bimetallic catalysts: The effect of Ni/Cu ratio on selectivity. *Applied Catalysis A: General* **2014**, *470*, 261-270.
- [31] Naghash, A.; Etsell, T.; Xu, S., XRD and XPS study of Cu- Ni interactions on reduced copper-nickel-aluminum: Oxide solid solution catalysts. *Chemistry of materials* **2006**, *18* (10), 2480-2488.
- [32] Yin, A.; Wen, C.; Guo, X.; Dai, W.-L.; Fan, K., Influence of Ni species on the structural evolution of Cu/SiO₂ catalyst for the chemoselective hydrogenation of dimethyl oxalate. *Journal of Catalysis* **2011**, *280* (1), 77-88.
- [33] Cheng, S.; Wei, L.; Zhao, X.; Julson, J., Application, Deactivation,

and Regeneration of Heterogeneous Catalysts in Bio-Oil Upgrading.

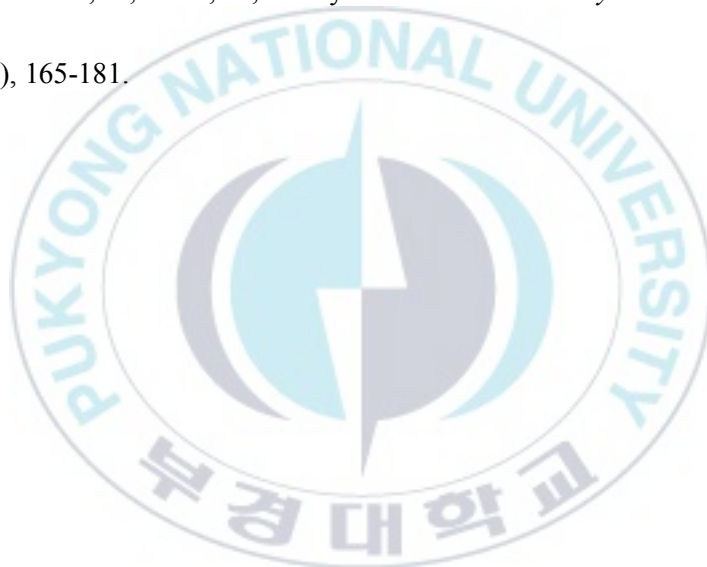
Catalysts **2016**, 6 (12), 195.

[34] Bartholomew, C. H., Mechanisms of catalyst deactivation. *Applied*

Catalysis A: General **2001**, 212 (1), 17-60.

[35] Forzatti, P.; Lietti, L., Catalyst deactivation. *Catalysis Today* **1999**,

52 (2), 165-181.



ACKNOWLEDGEMENT

First of all, I would like to express my deepest gratitude to my adviser, professor Hee Chul Woo for his encouragement, invaluable guidance and financial support throughout the period of my master course.

I would like to thank the appraiser committee members of my thesis, professor Jun Heok Lim and professor Jay Liu. Thanks for their brilliant and helpful comments and suggestions.

I wish to express my sincere thanks to the members of our laboratory who named Seong Chan Lee, Yong Beom Park and Hyeon Woo Oh. Their help and friendship have supported me a lot.

Finally, I would like to express my warmest gratitude to my parents for their unconditional support and wish them have good health and long life.